

Multi-modal estimation of the properties of containers and their content: survey and evaluation

Alessio Xompero, Santiago Donaher, Vladimir Iashin, Francesca Palermo, Gökhan Solak, Claudio Coppola, Reina Ishikawa, Yuichi Nagao, Ryo Hachiuma, Qi Liu, Fan Feng, Chuanlin Lan, Rosa H. M. Chan, Guilherme Christmann, Jyun-Ting Song, Gonuguntla Neeharika, Chinnakotla Krishna Teja Reddy, Dinesh Jain, Bakhtawar Ur Rehman, Andrea Cavallaro

Abstract—Acoustic and visual sensing can support the contact-less estimation of the weight of a container and the amount of its content when the container is manipulated by a person. However, transparencies (both of the container and of the content) and the variability of materials, shapes and sizes make this problem challenging. In this paper, we present an open benchmarking framework and an in-depth comparative analysis of recent methods that estimate the capacity of a container, as well as the type, mass, and amount of its content. These methods use learned and handcrafted features, such as mel-frequency cepstrum coefficients, zero-crossing rate, spectrograms, with different types of classifiers to estimate the type and amount of the content with acoustic data, and geometric approaches with visual data to determine the capacity of the container. Results on a newly distributed dataset show that audio alone is a strong modality and methods achieves a weighted average F1-score up to 81% and 97% for content type and level classification, respectively. Estimating the container capacity with vision-only approaches and filling mass with multi-modal, multi-stage algorithms reaches up to 65% weighted average capacity and mass scores.

I. INTRODUCTION

PEOPLE interact daily with household containers, such as cups, drinking glasses, mugs, bottles and food boxes. Methods to estimate the physical properties (e.g. weight and shape) of these containers could support human-robot cooperation. A robot should be able to predict these properties on-the-fly, for example while a container is manipulated by a human prior to a handover [1]–[5]. Methods should generalize to unknown container instances and use limited prior knowledge, such as generic categories of containers and contents [1], [6], [7]. However, the material, texture, transparency and shape vary considerably across containers and may change with the content. Furthermore, the content may not be visible due to the opaqueness of the container or because of occlusions.

A. Xompero, S. Donaher, F. Palermo, G. Solak, C. Coppola, and A. Cavallaro are with Centre for Intelligent Sensing, Queen Mary University of London, UK, {a.xompero, s.donaher, f.palermo, g.solak, c.coppola, a.cavallaro}@qmul.ac.uk. V. Iashin is with Tampere University, Finland, vladimir.iashin@tuni.fi. R. Ishikawa, Y. Nagao, and R. Hachiuma, are with Keio University, Japan {reina-ishikawa, soccerbass03, ryo-hachiuma}@keio.jp. Q. Liu, F. Feng, C. Lan, and R. H. M. Chan are with City University of Hong Kong, {qi.liu, fan.feng, cllan2-c, rosachan}@cityu.edu.hk. G. Christmann and J. T. Song are with National Taiwan Normal University, Taiwan, {guichristmann, ralphydineen}@gmail.com. G. Neeharika, C. K. T. Reddy, are with IIT Bhubaneswar, India, {gn12, ck13}@iitbbs.ac.in. D. Jain, is with IIT Hyderabad, India, ee17mtech11005@iith.ac.in. B. Rehman, is with miftah.ai, Pakistan, rehman.s.285@gmail.com.

Sensing modalities used to estimate the physical properties of containers and their content include RGB images, depth, thermal, haptic, and audio. These modalities can be used independently or jointly. The combination of modalities helps to overcome challenges faced by a single modality: for example, depth may be highly inaccurate with transparent objects [8]. When the content or container is manipulated, visual data can be complemented by acoustic data to predict the fullness of a container [1], [7], [9], [10]. Existing approaches mainly focus on estimating the level of the liquid, for example during the process of pouring the liquid in a container standing on a surface [6], [9], [11]–[13]. In addition to estimating the liquid level via regression or classification, several works visually estimate the pose, shape, and size of the container to support a handover [8], [14]–[20]. However, recognizing the amount and type of multiple materials - not limited to liquids - has been poorly investigated [7], [10], [21]–[23]. This is also the case for other properties of containers, such as their capacity and mass, the mass of the content, and the overall weight of the object (i.e., the container with its content).

To address these limitations, we present a novel, open framework for the estimation of the physical properties of a range of household containers and their content, when a person manipulates the container. The main tasks are the estimation of the capacity of the container, the type and amount of content, and the mass of the content. We refer to the amount of content as *filling level* and to the type of content as *filling type*. After reviewing the literature for filling level estimation (Sec. II), filling type estimation (Sec. III), and for the estimation of the capacity of the container (Sec. IV), we present the proposed framework, which includes a dataset, three tasks and related performance benchmarking measures (Sec. V). Using the proposed framework, we carry out an in-depth comparative analysis of state-of-the-art uni-modal and multi-modal methods (Sec. VI). Finally, we draw conclusions and discuss future research directions based on the experience of an international benchmarking challenge¹ organized using the proposed framework (Sec. VII).

II. FILLING LEVEL ESTIMATION

Determining the filling level of a container is often addressed with a single modality, such as visual, depth, or acoustic data. We discuss existing methods in terms of their

¹<https://corsmal.eecs.qmul.ac.uk/challenge.html>

modalities, features and approach to the problem, and if the methods consider different filling types (liquids and granular materials) and the manipulation of the container by a person.

Tracking a liquid state with a maximum a posteriori filter – e.g., the amount of water in an opaque container during a pouring task – is done by combining a physics-based model in a closed-loop simulator with real-time perception from RGB images to reduce the gap between reality and simulator [12]. The level of unknown liquids (e.g., milk, orange juice) is regressed by exploiting both the RGB image and the refraction of the liquid in the depth data, followed by a Kalman filter [24]. Edges can be detected in the RGB image and then associated to the height from the depth data. These features are then used together with Snell’s law to track and monitor the level of a liquid that a robot autonomously pours into a glass [11]. Alternatively, there are methods that quantize the filling level spectrum into a set of classes and perform classification instead of regression, using CNNs and a single-view RGB image [7], [9]. Fine-tuning the parameters of a CNN pre-trained on a large image dataset helps to overcome the limited availability of data for such a task [9], and the combination with adversarial training on the large dataset improves the generalization of the CNN to new images from different containers [7]. To overcome the presence of multiple containers in a scene, instance segmentation [25] can be used to identify each container prior to the classification of the object properties [7], [9]. Moreover, contextual information from the image can be used to improve the classification accuracy [9].

Manipulating a container generates sounds that can be exploited for the filling level estimation, especially when visual data is not available or the accuracy is low [26]–[28]. Examples are the variations in the volume of the air within a container [13], the vibration of acoustic waves [27] during a pouring process, or the frequency in the sound generated when a robot shakes and pours granular materials (coffee beans, rice, pasta, peat topsoil, plastic beads) with a scoop from and into a tub [28]. The height of the remaining air column in a container (e.g., glass cup, thermo, mug) is regressed during the mechanical pouring of a liquid (water, juice) with a RNN based on the Long Short-Term Memory (LSTM) unit and using audio signals converted into spectrograms [13]. Moreover, conditioning on both audio and force/torque data helps to handle noisy scenarios, improve the accuracy, and generalize to novel containers that are different in material and size [6]. These works, however, do not consider containers that are handled and manipulated by a person, introducing variations in the sound and hence failing to meet the assumptions. As for visual data, instead of regressing the precise filling level, the problem can be tackled as an audio classification task [29]–[31], considering a set of filling levels [10], [21]–[23]. Many-to-one sequence classification is performed using CNNs and a RNN with a LSTM unit or Gate Recurrent Unit (GRU) from multi-channel or mono-channel audio signals that are post-processed with Short-Term Fourier Transform (STFT) to obtain, e.g., log-Mel spectrograms as acoustic features [21], [22]. Alternatively, one-to-one sequence classification can be done by using one or multiple CNNs and spectrograms as

input features [10]. More traditional acoustic features can also be used individually or combined as input to classic machine learning classifiers, including k-Nearest Neighbour (kNN) [32], Support Vector Machine (SVM) [33], Random Forest (RF) [34], and Multi-layer Perceptron (MLP), for direct classification. Examples of features from short-term windows are Mel-Frequency Cepstrum Coefficients (MFCC), spectral characteristics, zero crossing rate (ZCR), chroma vector and deviation. Long-term features can be obtained by summarizing the short-term features from longer windows of the input audio signal, while including additional statistics, such as mean and standard deviation. When using multiple classifiers, each classifier can be trained in such a way that it is specialized to some specific data or sub-tasks [10], [23]. For example, MLPs can be trained on data specific only to each object category (*cup, drinking glass, food box*) [23], or a CNN can be trained to first recognize the manipulation performed by the person and other CNNs are trained specifically for the type of manipulation (e.g., shaking or pouring) [10]. The former can be achieved by also using visual data and an object detector to recognize the container in the frames of multiple image sequences followed by a majority voting. The voted category determines which specialized MLP is used for the filling level classification, using audio as input [23].

Multi-modal methods help to estimate the filling level when a modality can help to overcome limitations or ambiguities of each individual modality, such as noisy scenarios, already filled containers with absence of sound, opaque containers, or occlusions. Acoustic and visual data are the most common modalities used independently for filling level estimation and hence their combination and fusion are the more natural way to design a multi-modal algorithm [21]. A spatio-temporal CNN, pre-trained for action recognition, can extract visual features within a fixed window of frames from the RGB sequences of multiple camera views. R(2+1)D is an example of such spatio-temporal CNN and is based on residual connections [35] and 18 (2+1)D convolutional layers that approximate 3D convolution by a 2D convolution (spatial) followed by a 1D convolution (temporal) [36]. Long temporal relation between these features can also be estimated by using a RNN with GRU. A late fusion strategy – e.g., by averaging the class probabilities outputted by multiple classifiers associated with different modalities – can be devised to consider the visual information from multiple image sequences and the acoustic information from previously mentioned approaches, such as handcrafted features with RF and learned features via CNN and GRU [21].

Tab. I summarizes the methods discussed in this section. The task has been addressed by uni-modal methods using either audio or video inputs, and often restricted to the pouring scenarios of liquids where the container was not manipulated by a person. Methods vary in their use of acoustic or visual features, as well as in the choice of the classifiers, with a dominance of deep learning models. On the contrary, strategies that fuse both modalities for this task are very limited and there is room of investigation for effectively exploiting their complementary is available.

TABLE I

METHODS FOR FILLING LEVEL ESTIMATION. KEY – A: AUDIO, R: RGB, D: DEPTH, H: HAPTIC, T: TASK, M: MANIPULATED CONTAINERS BY A PERSON, L: LIQUIDS, G: GRANULAR MATERIALS, C: CLASSIFICATION, R: REGRESSION, CNN: CONVOLUTIONAL NEURAL NETWORK, MLP: MULTI-LAYER PERCEPTRON, TL: TRANSFER LEARNING, AT: ADVERSARIAL TRAINING, LSTM: LONG-SHORT TERM MEMORY, GRU: GATE RECURRENT UNIT, KF: KALMAN FILTER, LR: LINEAR REGRESSION.

Ref.	A	R	D	H	Approach	T	M	L	G
[12]	○	●	○	○	Open/closed-loop liquid simulator	R	○	●	○
[11]	○	●	●	○	Refracted D + KF	R	○	●	○
[24]	○	●	●	○	Edges + height (D) + Snell's law	R	○	●	○
[9]	○	○	○	○	CNN + TL	C	●	○	○
[7]	○	●	○	○	CNN + AT + TL	C	●	●	●
[28]	●	○	○	○	Spectrogram + LR/CNN/LSTM	R	○	○	●
[13]	●	○	○	○	Spectrogram + LSTM	R	○	●	○
[6]	●	○	○	●	Spectrogram + LSTM	R	○	○	○
[10]*	●	○	○	○	Spectrogram + kNN/SVM/RF	C	●	●	●
[10]*	●	○	○	○	Spectrogram + CNN	C	●	●	●
[10]*	●	○	○	○	Spectrogram + Hierarchy of 3 CNNs	C	●	●	●
[22]	●	○	○	○	Spectrogram + CNN + LSTM	C	●	●	●
[23]	●	●	○	○	object-specific MLP** R(2+1)D+GRU, CNN+GRU,	C	●	●	●
[21]	●	●	○	○	MFCC+SC+ZCR+CVS+RF, Late fusion (averaging)	C	●	●	●

*Joint classification of filling type and level with mono-channel audio

**Selected via object detection and majority voting

III. FILLING TYPE ESTIMATION

General food recognition using visual information is a well-investigated problem [37]–[39]. Recognizing the filling type within a container while being manipulated by a person is, however, a task that is not yet well-investigated and modalities beyond visual are usually not considered. Audio is an important modality that can carry relevant information about the filling type during manipulation and hence ease the recognition under certain conditions [10], [21], [22].

Classification of the filling type can be performed with a many-to-one sequence and a late fusion strategy by using both handcrafted and learned features extracted from input audio signals [21]. Handcrafted features, such as MFCC or ZCR, result from short-term windows of the spectral representation of a mono audio signal, and their summarization from a larger portion of the signal. If available, multi-channel instead of mono-channel signals can be used to improve the classification [22]. These long-term handcrafted features are then provided as input to a RF classifier. CNNs [35], [40] can extract learned features from a spectrogram representation (e.g., log-Mel spectrogram) of the signal, while a RNN with GRU handles the intrinsic temporal relations of the signals via a sliding window [21], [22]. The probabilities resulting from the last hidden state of the GRU network and those resulting from the RF are averaged to recognize the final class of the filling type [21]. Instead of capturing the temporal relations with a RNN, a majority voting strategy can be used across the CNN classification predictions of all windows [22]. Multiple specialized classifiers can be devised based on the category of a container (e.g., a drinking glass and a food box) [23]. In this case, visual data can be exploited to first determine the object category with a detector and a majority voting strategy to handle all the detected objects in an image sequence, and then a selected MLP classifies the filling type using an audio

TABLE II

METHODS FOR FILLING TYPE CLASSIFICATION OF MANIPULATED CONTAINERS. KEY – A: AUDIO, R: RGB, CNN: CONVOLUTIONAL NEURAL NETWORK, MANIP.: MANIPULATED CONTAINERS BY A PERSON, SPECT.: SPECTROGRAM, LSTM: LONG-SHORT TERM MEMORY, GRU: GATE RECURRENT UNIT, MLP: MULTI-LAYER PERCEPTRON.

Ref.	A	R	Features	Classifier	Fusion
[10]*	●	○	reshaped spect.	kNN/SVM/RF	–
[10]*	●	○	Spectrogram	CNN	–
[10]	●	○	Spectrogram	Hierarchy of 3 CNNs	–
[22]	●	○	multi-channel spect.	CNN + majority voting	–
[21]	●	○	MFCC+SC+ZCR+CVS RF, CNN+GRU		Late (avg)
[23]	●	●	Spectrogram	object-specific MLP**	–

*Joint classification of filling type and level

**Selected via object detection and majority voting

signal converted into a spectrogram [23].

On one hand, the filling type and level can be estimated independently, especially when only one of the two properties is necessary for the target application. On the other hand, the two properties are also correlated and if both properties are needed to be estimated, a joint estimation could be more desirable to unfeasible cases [10]. For example, using independent classifiers could lead to infeasible estimates, such as an *empty* filling level and *juice* as filling type, or *half-full* as filling level and *empty* as filling type. If these properties are also used for later estimates, such as the total object weight, then their wrong independent predictions could lead to large inaccuracies in the final estimation. While defining a set of seven feasible combinations of filling type and level based on the categories provided by a specific dataset [41], a direct classification of the joint class can be designed. From the observation that different containers can be manipulated in different ways, the problem can also be decomposed into two steps, namely action recognition and content classification, and three independent CNNs can be designed to take audio spectrograms as input [10]. The first CNN (action classifier) identifies the manipulation performed by the human, i.e., shaking or pouring, and the other two CNNs are task-specific and determine the filling type and level. The choice of which task-specific network should be used is conditioned by the decision of the first CNN. When the action classifier does not distinguish between pouring or shaking, the approach associates the *unknown* case to the class *empty*.

Tab. II summarizes the methods discussed in this section. Audio is the main modality considered for addressing this task with different choices among the classifiers, ranging from standard machine learning models to deep learning models. Temporal variations when using shorter windows on the input modality are handled with RNN models or a majority voting strategy. The main limitation is the range of materials that these models can be trained on, as large and diverse datasets are not available. Moreover, filling type and level estimation can benefit from each other to avoid unfeasible solutions, when both properties are required. However, one limitation of using only audio is that models cannot determine the correct filling type when a container is already filled and no manipulation is performed but it is simply picked up in real-world scenarios.

IV. CAPACITY ESTIMATION

The related literature mainly focuses on object recognition, object shape and size reconstruction in 3D, as well as pose estimation of a variety of objects using visual data [18]–[20], [25], [42], [43]. Sample containers are usually included and properties, such as transparency, are tackled on their own with ad-hoc designed approaches [8], [14], [17], [44]. Understanding higher level properties, such as the capacity of a household container, is an application-specific problem that is poorly investigated, and the main modalities considered as input are visual and depth data [9], [21]–[23], [45]. We discuss existing methods in terms of input modalities, adopted approach, manipulation, number of views, and the way the task is addressed (e.g., classification, regression, or geometric).

A CNN [35], [40], which is pre-trained on a large image dataset [46] and then fine-tuned on a smaller dataset specific for the task, can be used to classify the capacity of containers for liquids using a single RGB image and a binary mask of the query container as input [9]. The continuous set of positive real numbers is quantized into a non-uniform set of 10 intervals, which is sufficient when there is no need of high precision in the estimation. On the contrary, addressing the problem as a regression task results in worse performance, while adding context information provides a marginal improvement [9]. However, exploiting the depth to localize the object from a frontal view and then regressing the container capacity by providing the region of interest (ROI) and its relative size to a CNN is more effective than using the RGB image [45]. During the manipulation and human-to-robot cooperation, it is also important to determine the most reliable ROI. As the person holding an object would naturally extend the arm towards the robot before a handover, this prior knowledge can be exploited to constrain the maximum depth (e.g., to a maximum of 700 mm) [45]. Alternatively, distribution fitting via Gaussian processes can be used to determine the container capacity using ROIs extracted from multiple frames and views in image sequences of a person manipulating the container [23]. Multiple multi-variate Gaussian functions are then modeled depending on the container categories.

Geometric-based approaches uses either RGB and depth data or multiple RGB images to approximate a 3D shape and as by-product inferring the capacity [21], [22]. The 3D point cloud obtained from the RGB-D data and a mask of the object can be approximated to a cuboid by finding the minimum and maximum values for each coordinate in 3D [22]. To avoid occlusions by the human hand during manipulation, only the frame with a single silhouette having the largest number of pixels is selected, while frames with multiple silhouettes are discarded to avoid ambiguities. After post-processing the point cloud with Isolation Forest [47] to handle inaccuracies in the segmentation, the capacity is computed from the cuboid sides in 3D and re-scaled by a factor that accounts for the number of 3D points sampled and projected into the object silhouette [22]. Cylindrical shapes consisting of sparse points in 3D can be hypothesized from the RGB images of a wide-baseline stereo camera and an energy-based minimization approach can be used to fit the points to the real

TABLE III

METHODS FOR CAPACITY ESTIMATION. KEY – R: RGB, D: DEPTH, CNN: CONVOLUTIONAL NEURAL NETWORK, TL: TRANSFER LEARNING, MANIP.: MANIPULATED CONTAINERS BY A PERSON, ROI: REGION OF INTEREST, PROJ.: PROJECTIVE, MINIM.: MINIMISATION, APPROX.: APPROXIMATION, R: REGRESSION, C: CLASSIFICATION, G: PROJECTIVE GEOMETRY.

Ref.	R	D	Approach	Task	Manip.	# views
[9]	●	○	Normalized bounding box size	R	○	1
[9]	●	○	CNN + TL + Context	C	○	1
[45]	●	○	ROI + bounding box size + CNN	R	●	1
[22]	●	●	point cloud + 3D cuboid approx.	G	●	1
[21]	●	○	energy minim. + 3D cylinder approx.	G	●	2
[23]	●	○	Gaussian processes	R	●	4

All methods localize the container with object detection or instance segmentation.

shape of the object as observed and constrained in the object masks of the two views [8], [21], [48]. The capacity of the container is then computed by parametrizing the shape with multiple radius and heights and approximating the shape to a perfect cylinder (volume formula of a cylinder and using the average radius). However, this approach assumes that objects are rotationally symmetric (e.g., bottles and drinking glasses) and stand upright. Therefore, the approach cannot work with household containers that have a different shape. Moreover, this approach assumes that the object is fully visible in both images and is texture-less to compute the centroid in each silhouette and then triangulate the two points in 3D. During the manipulation, this assumption does not often hold and hence multiple estimations across frames can be used to improve the final estimation (e.g., averaging) [21].

Tab. III summarizes the main methods discussed in this section. Despite the different approaches or used modalities as input, these methods can be highly affected by the limited visibility of the container during manipulation or failures in localizing the container in the image due to the transparent material or severe occlusions by the human hand.

V. BENCHMARKING FRAMEWORK

A. Containers, fillings, scenarios

CORSMAL Containers Manipulation [41] is a dataset consisting of 1,140 audio-visual recordings with 12 human subjects manipulating 15 containers, split into 5 cups, 5 glasses, and 5 food boxes. These containers are made of different materials, such as plastic, glass and cardboard. Each container can be empty or filled with water, rice or pasta at two different levels of fullness: 50% and 90% with respect to the capacity of the container. The combination of containers and fillings results in a total of 95 configurations acquired for three scenarios with an increasing level of difficulty caused by occlusions or subject motions.

In the first scenario, the subject sits in front of the robot, while a container is on a table. The subject either pours the filling into the empty container, while avoiding touching the container, or shakes an already filled food box. Afterwards, the subject initiates the handover of the container to the robot. In the second scenario, the subject sits in front of the robot, while holding a container before starting the manipulation. In the third scenario, a container is held by the subject while standing

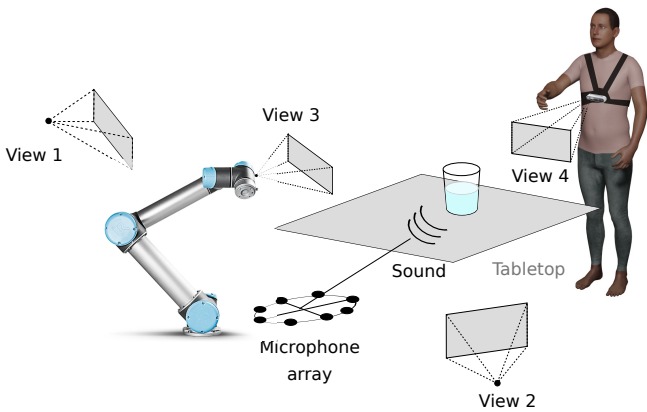


Fig. 1. The multi-modal, multi-sensor system used to record a person manipulating a container and its content. The system includes two third-person view cameras (at the two sides of the robot), a first-person view camera mounted on the robot, a first-person view from the body-worn camera on the person and a 8-microphone circular array (placed next to the robot arm).

to the side of the robot, potentially visible only on the third-person camera view. After the manipulation, the subject takes a few steps and initiates the handover of the container in front of the robot. Each scenario is recorded with two different backgrounds and under two different lighting conditions. The first background condition involves a plain tabletop with the subject wearing a texture-less t-shirt, while the second background condition involves the table covered with a graphics-printed tablecloth and the subject wearing a patterned shirt. The lighting conditions include ceiling room lights and controlled lights. Each subject executed the 95 configurations for each scenario and for each background/illumination condition².

B. Sensor data and annotation

The dataset was acquired with 4 multi-sensor devices, Intel RealSense D435i, and an 8-element circular microphone array (see Fig. 1). Each D435i device consists of 3 cameras and provides spatially aligned RGB, narrow-baseline stereo infrared, and depth images at 30 Hz with 1280x720 pixels resolution. In addition to the cameras, the device is equipped with an inertial measurement unit providing accelerometer and gyroscope information. One D435i is mounted on a robot arm that does not move during the acquisition and provides a more realistic view of the operating area from the robot perspective. Another D435i is worn by the person at chest level to provide a first-person view, while the remaining two devices are placed at the sides of the robot arm as third-person views that look at the operating area. The microphone array is placed on a table and consists of 8 Boya BY-M1 omnidirectional Lavelier microphones arranged in a circular shape of radius 15 cm. Audio signals are sampled synchronously at 44.1 kHz with a multi-channel audio recorder. All signals are software-synchronized with a rate of 30 Hz. The calibration information (intrinsic and extrinsic parameters) for each D435i and the inertial measurements of the D435i used as body-worn camera are also provided.

²Ethical approval (QMREC2344a) was obtained at Queen Mary University of London, and consent from each person was collected prior to data collection.

TABLE IV
THE MASS OF OBJECTS (CONTAINER AND FILLING) IN THE TRAINING SPLIT OF THE CCM DATASET, AND THE CAPACITY (CAP.) OF EACH CONTAINER. THE CLASS EMPTY CORRESPONDS TO THE MASS OF THE CONTAINER, WHICH IS KNOWN. KEY – CX: CONTENT TYPE (C) AND LEVEL (X), WHERE C CAN BE PASTA (P), RICE (R), OR WATER (W); AND X CAN BE HALF-FULL (5) OR FULL (9).

	Empty	2	3	10	15	86	134	15	31	59
Mass (g)	P5	37	39	119	37	131	205	104	297	776
	P9	65	69	205	54	175	262	174	509	1350
	R5	78	85	232	68	208	280	208	633	1548
	W5	95	104	270	79	234	316			
	R9	139	151	409	110	305	396	362	1115	2739
	W9	169	185	478	130	352	461			
Cap. (mL)	185	202	520	128	296	363	472	1240	3209	

The annotation of the data includes the capacity of the container, the filling type, the filling level, the mass of the container, the mass of the filling, the maximum width and height (and depth for boxes) of each object. Tab. IV reports the total object mass (container and filling masses) and the container capacity.

For validation, the dataset is split into train set (recordings of 9 containers), public test set (recordings of 3 containers), and private test set (recordings of 3 containers). The containers for each set are evenly distributed among the three categories. The annotations of the capacity of the container, filling type and level, and the mass of the container and filling are provided publicly only for the training set.

C. Tasks

We define three tasks, namely filling level classification (Task 1), filling type classification (Task 2) and container capacity estimation (Task 3). In Task 1, a container is either empty or filled with an unknown content at 50% or 90% of its capacity. For each recording related to a container, the goal is to classify the filling level. There are three classes, $\Lambda = \{empty, half-full, full\}$. In Task 2, containers are either empty or filled with an unknown content. For each recording related to a container, the goal is to classify the type of filling, if any. There are four filling type classes, $\mathcal{T} = \{empty, pasta, rice, water\}$. In Task 3, containers vary in shape and size. For each recording related to a container, the goal is to estimate the capacity of the container, γ .

The weight of the object is the sum of the mass of the (empty) container, m_c , and the mass of the (unknown) filling, m_f , multiplied by the gravitational earth acceleration, $g = 9.81 \text{ m/s}^{-2}$,

$$m = (m_c + m_f)g. \quad (1)$$

While we do not require the mass of the empty container to be estimated, we expect methods to estimate the capacity of the container and to determine the type and amount of filling to estimate the mass of the filling. For each recording related to a container, we then compute the filling mass as

$$\tilde{m}_f = \tilde{\lambda}\tilde{\gamma}D(\tilde{\tau}), \quad (2)$$

where $\tilde{\lambda} \in \Lambda$, $\tilde{\tau} \in \mathcal{T}$, and $D(\cdot)$ selects a pre-computed density based on the classified filling type. The density of pasta and rice is computed from the annotation of the filling mass, capacity of the container, and filling level for each container. Density of the water is 1 g/mL.

D. Performance measures

For the tasks of filling level classification and filling type classification, we compute precision, recall, and F1-score for each class n across all the configurations belonging to class n , S_n . *Precision* is the number of true positives over the total number of true positives and false positives for each class n (P_n). *Recall* is the number of true positives over the total number of true positives and false negatives for each class n (R_n). *F1-score* is the harmonic mean of precision and recall, defined as

$$F_n = 2 \frac{P_n R_n}{P_n + R_n}. \quad (3)$$

We then compute the weighted average F1-score, \bar{F}_1 , across the N classes, weighted by the number of configurations in class n , S_n ,

$$\bar{F}_1 = \frac{1}{S} \sum_{n=1}^N S_n F_n, \quad (4)$$

with $S = \sum_{n=1}^N S_n$ being the total number of recordings. Note that $N = 3$ for filling level classification, while $N = 4$ for filling type classification.

For capacity estimation, we compute the relative absolute error between the estimated capacity, $\hat{\gamma}_c^j$, and the annotated capacity, γ_c^j , for each configuration, j , of container c ,

$$\epsilon_c^j = \frac{|\hat{\gamma}_c^j - \gamma_c^j|}{\gamma_c^j}. \quad (5)$$

For filling mass estimation, we similarly compute the relative absolute error between the estimated, $\hat{m}_{f,c}^j$, and the annotated filling mass, $m_{f,c}^j$, for each configuration, j , of container c , unless the annotated mass is zero (empty filling level),

$$\epsilon_j^c = \begin{cases} 0, & \text{if } m_{f,c}^j = 0 \wedge \hat{m}_{f,c}^j = 0, \\ \hat{m}_{f,c}^j, & \text{if } m_{f,c}^j = 0 \wedge \hat{m}_{f,c}^j \neq 0, \\ \frac{|\hat{m}_{f,c}^j - m_{f,c}^j|}{m_{f,c}^j}, & \text{otherwise.} \end{cases} \quad (6)$$

We then compute the average capacity score, \bar{C} , as

$$\bar{C} = \frac{1}{S} \sum_{c=1}^C \sum_{j=1}^{S_c} \mathbb{1} e^{-\epsilon_c^j}, \quad (7)$$

where S_c is the number of configurations with container c . We similarly compute the average filling mass score, \bar{M} . Note that estimated and annotated capacities (masses) are strictly positive, $\hat{\gamma}_c^j > 0$ and $\gamma_c^j > 0$. The indicator function $\mathbb{1} \in \{0, 1\}$ is 0 only when the capacity (mass) of the container c in recording j is not estimated.

VI. COMPARATIVE ANALYSIS

To evaluate methods on the tasks described in the previous section, we organized an open challenge. In this section we discuss the methods that competed in the challenge as well as baseline methods. The methods are *Challengers*, *NTNU-ERC* (NTNU) [45], *VA2Mass* (VA2M) [23], *HVRL* [22], and *Because It's Tactile* (BIT) [21]. We also include a recently submitted audio-only based approach for the joint classification of content type and level (ACC) [10].

A. Implementation details

Challengers uses audio data to classify filling type and filling level with a fully connected neural network. After suppressing the noise in each audio signal via spectral gating, Challengers computes the STFT from the signal and uses it as input feature for a classifier based on a 5-layer fully connected neural network, trained with ADAM optimizer [49] and dropout [50] on the last layer to reduce overfitting.

NTNU uses audio as the input modality for filling type classification and extracted 40 normalized MFCC features in a window size of 20 ms at 22 kHz, with a maximum length of 30 s. NTNU uses zero-padding to preserve the same duration across audio data. The MFCC features of all frames are concatenated in a $40 \times 1,501$ matrix. The matrix is provided as input to a CNN that consists of 2 convolutional layers and 1 fully connected layer, resulting in 86,876 trainable parameters. The CNN is trained with SGD optimizer, a fixed learning rate of 0.00025 and momentum of 0.9, and a batch size of 16. For estimating the container capacity, the ROI containing the object is extracted by finding the contour features in a binary mask created from a depth image. The ROI and the normalized relative size are then provided as input to another CNN consisting of 4 convolutional layers, each followed by batch normalization [51], and 3 fully connected layers. This CNN has 532,175 trainable parameters.

VA2M uses YOLOv4 [52], pre-trained on the MS COCO dataset [53], to detect the object in each frame of the videos from the four camera views. The class category is determined by a majority voting of the three categories (*cup*, *drinking glass*, *food box*) recognized by YOLOv4. The majority voting is performed by using frames randomly sampled in each RGB video of the training split of CORSMAL Containers Manipulation (65% of all frames). For the tasks of filling type and filling level classification, VA2M uses 3 specialized MLP classifiers, each trained on audio data belonging to a specific container category. Each MLP has 3 layers with 3,096 nodes in the first hidden layer and 512 in the last hidden layer. The total number of trainable parameters is 20,762,288. Multi-channel audio recordings are re-sampled at 16,600 Hz and converted into mono-channel by averaging the samples across channels. Only the last 32,000 samples are retained and converted into spectrogram as audio feature via Discrete Fourier Transform. For capacity estimation, VA2M models the distribution of each container category as Gaussian function and then regresses the capacity with a Gaussian process, using the container type and sampled bounding boxes as input. The output is the capacity value of each sample.

HVRL uses all the 8 audio signals from the microphone array to compute log Mel-scaled spectrogram with STFT and 64 filter banks for filling type and filling level classification. For the STFT, HVRL sets the frame length to 25 ms, the hop-length of 10 ms, and the number of samples for the Fast Fourier Transform to 512. To handle audio signals of different duration and re-size them to a fixed duration, HVRL adds zero-padding when the audio signals are shorter than 100 audio frames, while longer audio signals are truncated to 100 audio frames from the beginning of the signals. During training, HVRL crops audio signals based on manual annotations (provided publicly) of the starting and ending of the manipulation. A sliding window on the cropped spectrogram with 75% overlap forms overlapping audio frames consisting of 3D tensors, where the third dimension is given by the 8 audio channels. Each window is provided as input to a CNN consisting of 5 blocks, each with 2 convolutional and 1 batch normalization layers followed by a max-pooling layer. The CNN is complemented by 3 fully connected layers for the filling type classification of each audio frame and followed by the majority voting. The CNN has a total of 13 layers with 4,472,580 trainable parameters. The same extracted features are also used as input to the three stacked LSTMs for the filling level classification. The three stacked LSTMs are trained with a set of 100 audio frames and contain 256 hidden states, resulting in 2,366,211 trainable parameters. The network is trained by using cross-entropy loss and ADAM optimizer [49] with a learning rate of 0.00001 and a mini-batch size of 32 for 200 epochs. For capacity estimation, HVRL uses RGB-D images to approximate the 3D point cloud to a cuboid. The capacity of the cuboid is then re-scaled by a factor that depends on the number of pixels within the mask of the object and the number of pixels within the area covered by the projected cuboid.

BIT converts a multi-channel audio signal into a mono-channel by averaging the samples across channels, and then computes MFCC, energy, spectral characteristics, and their statistics from 50 ms windows of the input signal. The features are concatenated in a 136-dimensional vector used as input to a RF classifier for filling level estimation. The number of trees of the RF classifier is automatically set during training by selecting the value between (10, 25, 50, 100, 200, 500) that achieves the highest accuracy in validation. BIT also computes a 128-dimensional vector of features by using a VGG-based model [54], pre-trained on the large AudioSet dataset [55]. After re-sampling a mono-channel audio signal at 16 kHz, BIT provides the mel-scale spectrograms extracted from 960 ms windows of the re-sampled signal to the VGG-based model as input. The learned features are then provided as input to a GRU model [56] that has 5 layers and a hidden layer of size 512. The model has a total of 7,291,395 trainable parameters. For filling level estimation, BIT also uses the visual modality from the RGB video recordings of the four camera views. For each video, visual features are first extracted as 512-dimensional vector by using $R(2+1)D$ [36], pre-trained on the Kinetics 400 action classification dataset [57] and whose input consists of 16 RGB frames of 112×112 pixel resolution. Each vector is then independently provided to a GRU model

that has 3 layers and a hidden dimension of size 512. Each GRU has a total of 4,729,347 trainable parameters. BIT jointly trained the four GRU models and summed their logits before applying the final softmax. The final prediction of the filling level is obtained by averaging the class probabilities of the RF classifier as well as the GRU models for both the audio and visual features. For filling type estimation, BIT uses only audio information as input and re-trained the RF classifier and the GRU model with 4 classes. The RF classifier and all the GRU models are trained by using 3-fold validation strategy on the training set of CORSMAL Containers Manipulation. For the capacity estimation, BIT uses 1st and 20th to the last RGB frames from left and right view cameras without pre-processing. Mask R-CNN [25] pre-trained on COCO [53] is used to detect a container for each frame by selecting the category the belongs either of five classes – *bottle*, *wine glass*, *cup*, *book*, *vase* – to resemble the objects in CORSMAL Containers Manipulation. The capacity of the container is then estimated from the image crop of the object and by using a multi-view energy minimization approach with a 3D cylinder hypothesis and approximation [8].

ACC consists of three independent CNNs: the CNN for action recognition (*pouring*, *shaking*, *unknown*) has 4 convolutional, 2 max-pooling, and 3 fully connected layers; the CNN for the specific action of pouring has 6 convolutional, 3 max-pooling, and 3 fully connected layers; and the CNN for the specific action of shaking has 4 convolutional, 2 max-pooling, and 2 fully connected layers. ACC includes a pre-processing step that down-samples the input sound signal to 22,050 Hz, normalizes it to [-1,1] to eliminate relative gain variations, and performs onset [58] detection to identify the beginning of an action. The method then transforms a temporal window of fixed duration (e.g., 10 s) from the onset to a spectrogram that is provided as input to each CNN.

The challenge also provided a range of uni-modal baselines that use only audio or only images as input data to solve the classification of filling level and filling type. For the 12 baselines using only audio as input modality, different types of features are computed from the signals and are provided as input to three classifiers, namely kNN, SVM, and RF. The features considered are spectrograms, ZCR, MFCC, chromogram, mel-scaled spectrogram, spectral contrast, and tonal centroid features (tonnetz). For MFCC, the 1st to 13th coefficients are used, while the 0th coefficient is discarded. Similar to the baselines for the environmental sound classification [29], three baselines use the mean and standard deviation of the MFCC and ZCR features across multiple audio frames. Other three baselines extract a feature vector consisting of 193 coefficients from the mean and standard deviation of the MFCC, chromogram, mel-scaled spectrogram, spectral contrast, and tonnetz across multiple audio frames. Three baselines are selected from the comparison in ACC's work [10], and they use the spectrograms computed as input to the CNN-based models of ACC and reshaped into a vector of dimension 9,216. In addition to these baselines, we include three baselines that perform dimensionality reduction with the Principal Component Analysis (PCA) method on the reshaped spectrograms to remove redundant and less relevant

information. The first 128 components are retained for these baselines. Similar to ACC, all these baselines classify filling type and level jointly.

The vision-only baseline uses two CNNs to perform independent classification of filling level and filling type from a single RGB image crop. The image crop is extracted from the last frame of an input video using Mask R-CNN [25] to select the segmentation mask with the most confident class between *cup* and *wine glass*. The classifiers are re-trained ResNet-18 architectures [35] using a subset of frames selected within the video recordings of the training set of the provided dataset [7]. The network includes an additional class, *opaque*, to handle cases where containers are not transparent and vision alone fails to determine the content type and level [7], [9].

B. Discussion

We compare the proposed methods and baselines, and we analyze the performance in terms of weighted average F1-score and confusion matrices for filling level and filling type classifications, individually. Note that we report and discuss the results in percentage for the scores.

Tab. V compares the performance of all methods except NTNU for filling level classification. ACC, BIT, and HVRL achieve the highest accuracy with 80.84, 79.65, and 78.65 \bar{F}_1 on the combined testing splits of the dataset, respectively. This performance is almost twice higher than VA2M and Challengers. Moreover, ACC and HVRL show that using only audio as input modality is sufficient to achieve an accuracy higher than 75 \bar{F}_1 . BIT is also using visual information from the RGB sequence of all the four camera views, but the performance similar to ACC and HVRL might imply that audio features are dominant in determining the classification decision. However, further inspections of the method isolating the modalities would be necessary to confirm whether audio is the dominant modality. While the three methods are close to each other, ACC is the best performing in the private split and the combined public and private testing splits. HVRL is the best performing in the public testing split with a \bar{F}_1 of 82.63. Interestingly, both methods selected a fixed portion of the audio signal, transformed into a spectrogram, where the manipulation of the container by the human subject was more likely to occur. However, ACC chose to provide the full portion as input to the three CNNs, whereas HVRL adopted a temporal approach consisting of a CNN and an LSTM. Both show to be valid methods assuming that the whole audio signal is available and the manipulation is completed.

Looking more in detail at the confusion matrices in Fig. 2, we can observe that ACC and HVRL do not confuse the class *empty*, while BIT mis-classifies some *empty* configurations as *half-full*. As expected, most of the confusions occur between the classes *half-full* and *full* for all methods. BIT and HVRL are more accurate than ACC in recognizing the class *half-full*, but ACC is more accurate in recognizing the class *full*. VA2M mis-classifies the true class *empty* as *half-full* for 40% of the times and as *full* for 33% of the times, and the class *full* is confused with *half-full* for 75% of the times. This is likely to be caused by the three MLP-based classifiers associated with

TABLE V
FILLING LEVEL CLASSIFICATION RESULTS (TASK 1). KEY – A: AUDIO, RX: RGB FOR VIEW X (1,2,3,4), ZCR: ZERO CROSSING RATE, MFCC: MEL-FREQUENCY CEPSTRUM COEFFICIENTS, RF: RANDOM FOREST, SVM: SUPPORT VECTOR MACHINE, KNN: K-NEAREST NEIGHBOUR, PCA: PRINCIPAL COMPONENT ANALYSIS, A5F: AUDIO 5 FEATURES (MFCC, CHROMOGRAM, MEL-SCALED SPECTROGRAM, SPECTRAL CONTRAST, TONAL CENTROID FEATURES).

Method	Input modalities				Testing splits			
	A	R1	R2	R3	R4	Public	Private	Overall
Random	–	–	–	–	–	33.35	41.86	37.62
Mask R-CNN + ResNet-18	○ ●	○ ○	○ ○	○ ○	○ ○	58.51	32.93	47.00
Mask R-CNN + ResNet-18	○ ○	○ ●	○ ○	○ ○	○ ○	48.90	26.73	39.00
Mask R-CNN + ResNet-18	○ ○	○ ○	○ ●	○ ○	○ ○	36.52	25.52	31.46
Mask R-CNN + ResNet-18	○ ○	○ ○	○ ○	○ ●	○ ○	25.12	21.99	23.68
ZCR + MFCC + kNN	● ○	○ ○	○ ○	○ ○	○ ○	63.63	54.97	59.35
ZCR + MFCC + SVM	● ○	○ ○	○ ○	○ ○	○ ○	66.27	57.19	61.87
ZCR + MFCC + RF	● ○	○ ○	○ ○	○ ○	○ ○	70.04	63.11	66.80
A5F + kNN	● ○	○ ○	○ ○	○ ○	○ ○	55.49	53.22	54.47
A5F + SVM	● ○	○ ○	○ ○	○ ○	○ ○	60.77	58.57	60.09
A5F + RF	● ○	○ ○	○ ○	○ ○	○ ○	64.18	63.94	64.74
Spectrogram + kNN	● ○	○ ○	○ ○	○ ○	○ ○	59.15	53.47	56.38
Spectrogram + SVM	● ○	○ ○	○ ○	○ ○	○ ○	47.66	51.54	49.67
Spectrogram + RF	● ○	○ ○	○ ○	○ ○	○ ○	45.43	45.59	45.49
Spectrogram + PCA + kNN	● ○	○ ○	○ ○	○ ○	○ ○	39.03	37.16	38.31
Spectrogram + PCA + SVM	● ○	○ ○	○ ○	○ ○	○ ○	30.08	31.99	31.64
Spectrogram + PCA + RF	● ○	○ ○	○ ○	○ ○	○ ○	46.79	42.46	44.66
VA2M [23]	● ●	● ●	● ●	● ●	● ●	44.31	42.70	43.53
Challengers	● ○	○ ○	○ ○	○ ○	○ ○	50.73	47.08	48.71
HVRL [22]	● ○	○ ○	○ ○	○ ○	○ ○	82.63	74.43	78.56
BIT [21]	● ●	● ●	● ●	● ●	● ●	78.14	81.16	79.65
ACC [10]	● ○	○ ○	○ ○	○ ○	○ ○	80.22	81.46	80.84

Best performing method highlighted in bold.

each container category and hence an error in the category choice may lead to a different decision by the classifier due to the limited and selected training data. Indeed, the recognition accuracy of the container categories *cup*, *drinking glass* and *food box* are 92%, 73%, and 88%, respectively, in the training split. The CNN of the team Challengers made erroneous predictions across all classes, except for *empty* that was never predicted as *half-full* but only confused with *full*. The vision-only baseline (using the first camera view, on the left side of the robot arm) confused 81% of the times the class *empty* with *half-full* in addition to mis-classification between *half-full* and *full*, making the performance of the baseline only 10 \bar{F}_1 higher than a random classifier (37.62 \bar{F}_1). Vision alone is a weak modality for the filling level classification problem due to the ambiguities caused by the transparency of the content (e.g., water) or the opacity of the container that does not allow a CNN to determine the amount of content inside when using only a single image. Moreover, contents such as pasta and rice at different levels as well as the occlusion caused by the human hand holding the container in the last frame can affect the segmentation of the container when using Mask R-CNN, leading to a wrong prediction of filling level.

Tab. VI compares the performance of all methods and baselines for filling type classification. As for filling level classification, HVRL, ACC, and BIT are the best performing with 96.95 \bar{F}_1 , 94.50 \bar{F}_1 , 94.26 \bar{F}_1 score on the combined testing splits. Audio is the chosen modality by all the methods except VA2M that also combines visual information. Using only audio is again sufficient to achieve performance close

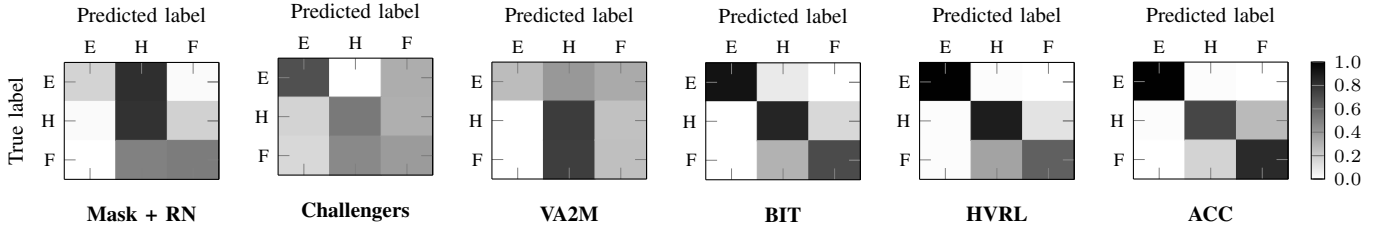


Fig. 2. Confusion matrices of filling level classification for all methods across all the containers of the public and private testing splits of the CORSMAL Container Manipulation dataset [41]. Note that the counting for each cell is normalized by the total number of true labels for each class (colorbar). KEY –E: empty; H: half-full; F: full, Mask + RN: Mask R-CNN + ResNet-18.

TABLE VI

FILLING TYPE CLASSIFICATION RESULTS (TASK 2). KEY – A: AUDIO, RX: RGB FOR VIEW X (1,2,3,4), ZCR: ZERO CROSSING RATE, MFCC: MEL-FREQUENCY CEPSTRUM COEFFICIENTS, RF: RANDOM FOREST, SVM: SUPPORT VECTOR MACHINE, KNN: K-NEAREST NEIGHBOUR, PCA: PRINCIPAL COMPONENT ANALYSIS, A5F: AUDIO 5 FEATURES (MFCC, CHROMOGRAM, MEL-SCALED SPECTROGRAM, SPECTRAL CONTRAST, TONAL CENTROID FEATURES).

Method	Input modalities					Testing splits		
	A	R1	R2	R3	R4	Public	Private	Overall
Random	–	–	–	–	–	21.24	27.52	24.38
Mask R-CNN + ResNet-18	○	●	○	○	○	30.85	13.04	23.05
Mask R-CNN + ResNet-18	○	○	●	○	○	28.75	15.54	22.90
Mask R-CNN + ResNet-18	○	○	○	●	○	21.14	9.04	15.63
Mask R-CNN + ResNet-18	○	○	○	○	●	14.12	11.23	12.70
ZCR + MFCC + kNN	●	○	○	○	○	88.19	79.23	83.73
ZCR + MFCC + SVM	●	○	○	○	○	84.23	71.96	78.67
ZCR + MFCC + RF	●	○	○	○	○	92.97	89.74	91.31
A5F + kNN	●	○	○	○	○	76.84	75.96	76.41
A5F + SVM	●	○	○	○	○	64.92	79.72	72.86
A5F + RF	●	○	○	○	○	88.36	87.46	87.88
Spectrogram + kNN	●	○	○	○	○	60.50	68.58	64.55
Spectrogram + SVM	●	○	○	○	○	39.39	41.81	40.61
Spectrogram + RF	●	○	○	○	○	47.98	47.68	47.82
Spectrogram + PCA + kNN	●	○	○	○	○	24.47	28.34	26.53
Spectrogram + PCA + SVM	●	○	○	○	○	20.57	27.60	24.20
Spectrogram + PCA + RF	●	○	○	○	○	28.75	37.79	33.32
VA2M [23]	●	●	●	●	●	41.77	41.90	41.83
Challengers	●	○	○	○	○	78.58	71.75	75.24
NTNU [45]	●	○	○	○	○	81.97	91.67	86.89
BIT [21]	●	○	○	○	○	93.83	94.70	94.26
ACC [10]	●	○	○	○	○	95.12	93.92	94.50
HVRL [22]	●	○	○	○	○	97.83	96.08	96.95

Best performing method highlighted in bold.

to 100 \bar{F}_1 score, whereas the baseline using only visual input achieves similar or lower \bar{F}_1 than a random classifier. If the audio modality was not available, both filling level and filling type classifications would be very challenging for methods using only visual data. We can also observe that visual data is also problematic for VA2M that also uses audio data. However, the lower performance could be caused again by the multiple MLP-based classifiers after the decision on the container category. The bottleneck on selecting which classifier to use might be the main source of error for the classifications. Indeed, we can notice that the performance is similar between the two tasks with 43.53 \bar{F}_1 and 41.83 \bar{F}_1 for filling level and filling type classification, respectively. Challengers and NTNU are also effective, achieving 75.24 \bar{F}_1 and 86.89 \bar{F}_1 , respectively, but lower of about 20 \bar{F}_1 and 10 \bar{F}_1 , respectively, than HVRL. We can also observe from

the table that the performance of the baselines varies from random results to almost the same performance as the best performing HVRL. Using the spectrogram as input feature (either after reshaping the spectrogram into a vector or after applying PCA to select the first 128 components) to any of the three classifiers, namely kNN, SVM, or RF, is the worst choice. On the combined testing splits, the lowest performance is obtained by Spectrogram + PCA + SVM with 24.20 \bar{F}_1 , while the highest performance is obtained by Spectrogram + kNN with 64.55 \bar{F}_1 . It is also surprising how a large feature vector resulting from the reshaped spectrogram leads to a reverse ranking of the three classifiers with kNN being the best performing. However, we do not currently have an explanation for this phenomenon and further inspections are needed. Classic audio features, such as MFCC and ZCR, are more discriminative and sufficient to achieve performance higher than 78 \bar{F}_1 for the three classifiers. On the contrary, performance decreases when using a larger set of features, such as tonal centroid, spectral contrast, chromogram, mel-scaled spectrogram, and MFCC. However, it is important to note that simply using ZCR and MFCC with RF can achieve 91.31 \bar{F}_1 , which is close to the performance of the three top methods (BIT, ACC, HVRL) that are using CNNs and LSTM.

Looking more in detail at the confusion matrices in Fig. 3, we can observe that HVRL made a few mis-classifications for the class *rice* with *empty* and *pasta*, and for the class *water* with *empty*. ACC confused 4% *pasta* with *rice*, 4% *rice* with *pasta*, 7% *pasta* with *water*, and 2% *water* with *empty*. While the confusion between *water* and *empty* could be expected due to the low volume of the sound produced by the water, the confusion of *water* with *rice* might be caused by the glass material of the container and noise background. The largest confusion for BIT is given by the erroneous prediction of *rice* with *pasta* (13%). As for filling level classification, VA2M and Challengers have large mis-classifications across different classes, with VA2M that could not predict *water* for any audio input.

For capacity estimation, we compare the results of HVRL, BIT, VA2M, and NTNU, in terms of the average capacity score. We also report the results of a pseudo-random generator (Random) that draws the predictions from a uniform distribution in the interval [50, 4000] based the Mersenne Twister algorithm [59]. We then analyze and discuss the statistics of the absolute error in predicting the container capacity for each testing container as well as for each filling type and level.

Tab. VII shows that NTNU achieves the best score with

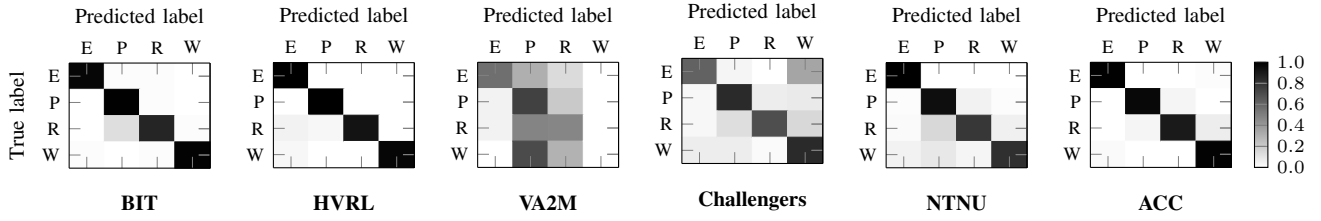


Fig. 3. Confusion matrices of filling type classification for all methods across all the containers of the public and private testing splits of the CORSMAL Containers Manipulation dataset [41]. Note that the counting for each cell is normalized by the total number of true labels for each class (colorbar). KEY –E: empty; P: pasta; R: rice; W: water.

TABLE VII
CONTAINER CAPACITY ESTIMATION RESULTS (TASK 3). KEY –
MX: MODALITY M FOR VIEW X (1,2,3,4), WHERE M IS EITHER RGB (R) OR
DEPTH (D).

Method	Input modalities								Splits		
	R1	D1	R2	D2	R3	D3	R4	D4	Public	Private	Overall
Random	-	-	-	-	-	-	-	-	31.63	17.53	24.58
HVRL [22]	●	●	○	○	○	○	○	○	57.19	52.38	54.79
BIT [21]	●	○	●	○	○	○	○	○	60.56	60.58	60.57
VA2M [23]	●	○	●	○	●	○	●	○	63.00	62.14	62.57
NTNU [45]	○	○	○	○	○	○	●	○	66.92	67.67	67.30

Best performing method highlighted in bold.

66.92 \bar{C} , 67.67 \bar{C} , and 67.30 \bar{C} for the public testing set, private testing set, and combined testing sets, respectively, when using only depth data from the fixed frontal view. All methods achieve a performance score that is twice higher than the random solution (24.58 \bar{C} for the combined testing sets): HVRL has the lowest score (54.79 \bar{C}), while BIT and VA2M obtain 60.57 \bar{C} and 62.57 \bar{C} , respectively. Fig. 4 shows the statistics (minimum, maximum, median, 25th and 75th percentiles) of the relative absolute errors for each container in the testing splits of the dataset. NTNU has the lowest median error for all containers, except for the private containers C14 and C15. The variation of the error across configurations is either smaller than the variation of the other methods or lower than the median value of the other methods. BIT is more consistent in estimating the same container shape and capacity for most of the configurations related to containers C12 and C15. BIT also have the largest variations for C10 and C14; VA2M for C12 and C15; and HVRL for C11. Interestingly, VA2M have a median error lower than HVRL and BIT for C13 and achieve the lowest median error with a small variation across configurations for C14. However, we can observe that in general the relative absolute error across containers is around or higher than 0.5. This makes capacity estimation the most challenging task, and large room of improvements for new methods is possible.

In addition to the comparison across containers, Fig. 5 shows the relative absolute errors grouped by filling type and level for each method. We can observe that most of the errors are in the interval [0.3,0.8], and the methods have similar amount of variations between the 25th and 75th percentiles, but differences are in the median error and the maximum error (excluding outliers). NTNU achieves the lowest median error (always lower than half of the real container capacity) and smaller variations (25th-75th percentiles), whereas VA2M have

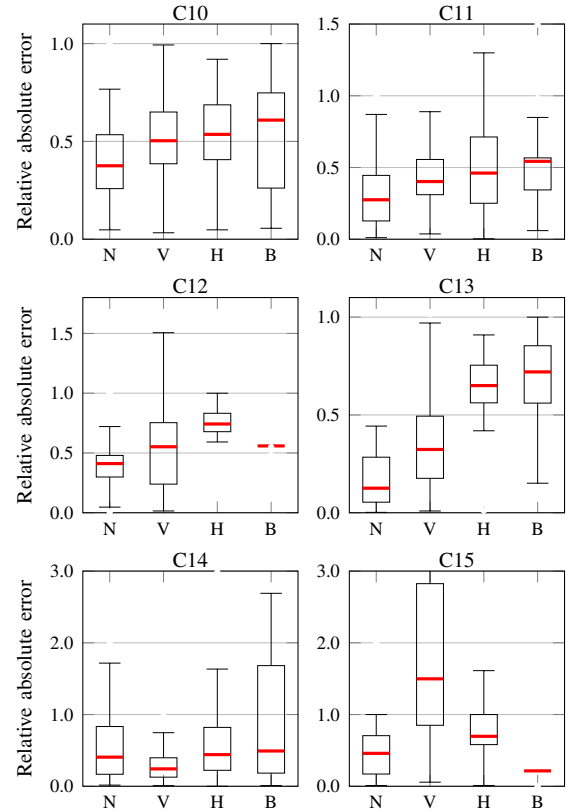


Fig. 4. Comparison of statistics of the absolute error in estimating the container capacity for each testing container between NTNU (N) [45], VA2M (V) [23], HVRL (H) [22], and BIT (B) [21]. Note that outliers in the data are not shown. Note also the different scale for the y-axis. KEY – CX: container (C) index (X), where X is in the range [10,15].

similar results for *rice full*. HVRL has the largest errors for *empty*, *pasta half-full*, *pasta full*, *rice half-full*, and *rice full*, whereas BIT has the largest errors for *water half full* and *water full*. Overall, we can conclude that the presence of the fillings at different amounts is not significantly affecting the estimation of the container capacity for the four methods. However, large errors still suggest that the task is difficult.

We also analyze the performance scores grouped by scenario and containers for all the three tasks in Tab. VIII. HVRL, BIT, and ACC increase their \bar{F}_1 for filling level classification on the testing containers from scenario 1 to scenario 3, showing how audio information is robust despite the increasing difficulty due to the in-hand manipulation (scenario 2 and 3) and larger distance (scenario 3). However, ACC decreases by almost 2 percentage points (pp) from scenario 1 (78.52 \bar{F}_1) to scenario 2

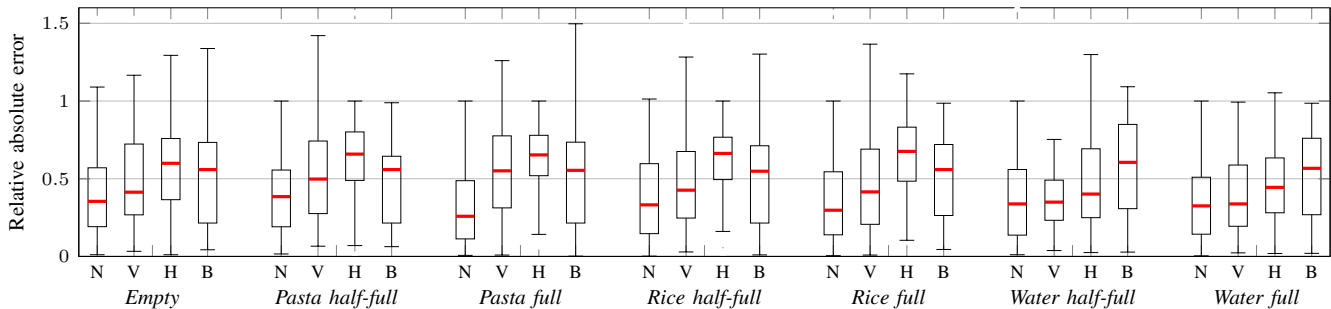


Fig. 5. Comparison of statistics of the absolute error in estimating the container capacity for each testing container between NTNU (N) [45], VA2M (V) [23], HVRL (H) [22], and BIT (B) [21].

(76.92 \bar{F}_1). On the contrary, Challengers is affected by the in-hand manipulation and distance, decreasing from 52.90 \bar{F}_1 in scenario 1 to 45.46 \bar{F}_1 in scenario 3. VA2M achieve the highest accuracy for scenario 2 (51.34 \bar{F}_1), increasing by 11.51 pp compared to scenario 1 (39.83 \bar{F}_1), but decreasing to 35.92 \bar{F}_1 in scenario 3. As explained earlier, this is likely to be linked to the errors in classifying the object category and hence the choice of the classifier, affecting the final prediction. For filling type classification, performance of HVRL, BIT, and ACC are higher than 90 \bar{F}_1 across the scenarios, but the trend is the opposite of filling level classification. BIT and ACC decrease in \bar{F}_1 from scenario 1 to scenario 3, while HVRL achieve the highest accuracy in scenario 2 (98.07 \bar{F}_1). VA2M and Challengers show the same behavior as for filling level and type with a large decrease in scenario 3 by 15.31 pp and 22.16 pp compared to scenario 1, respectively. For capacity estimation, VA2M and HVRL are less affected by the variations across the scenarios, while NTNU is the best performing in scenario 1 (68.81 \bar{C}) and scenario 2 (73.70 \bar{C}) but decreases by 9.42 pp in scenario 3 compared to scenario 1. NTNU is based only on the frontal depth view, where the subject is not visible for most of the time. This challenges the method to detect the object in the pre-defined range. BIT is affected by the increasing challenges across scenarios decreasing from 66.51 \bar{C} in scenario 1 to 55.68 \bar{C} in scenario 3. This shows the limitations of the underline approach [8] that was designed for objects free of occlusions and standing upright on a surface.

The performance across containers varies between the methods. Testing containers 12 and 15 are the most challenging for VA2M, HVRL, BIT, ACC, when classifying the filling level, while Challengers achieves its best performance on the same containers. HVRL and BIT have the largest decrease with the score in the interval [40,50] \bar{F}_1 compared to the interval [75-93] \bar{F}_1 for the other containers. ACC outperforms all the other methods with 64.98 \bar{F}_1 and 74.99 \bar{F}_1 for containers 12 and 15. For filling type classification, VA2M obtains 86.98 \bar{F}_1 and 79.45 \bar{F}_1 for containers 12 and 15, respectively, while achieving less than 30 \bar{F}_1 on the other containers. Given the structured organization of the sets of recording per containers in the challenge, it is clear that VA2M can recognize the *box* class and the filling type for that class, but the method cannot easily distinguish filling type and level for drinking glasses and cups. Overall, other methods achieve a score higher than 70 \bar{F}_1 across containers. HVRL achieves 100 \bar{F}_1 on container 13 and ACC on container 15. HVRL is the best performing

TABLE VIII
COMPARISON OF THE TASK PERFORMANCE SCORES BETWEEN METHODS FOR EACH SCENARIO AND FOR EACH TESTING CONTAINER. KEY – S: SCENARIO, C: CONTAINER, T: TASK.

Method	S1	S2	S3	C10	C11	C12	C13	C14	C15
VA2M [23]	39.83	51.34	35.92	35.24	36.59	22.86	33.74	33.74	26.33
Challengers	52.90	47.37	45.46	48.69	46.78	58.27	41.43	38.89	62.58
T1									
HVRL [22]	75.41	77.70	82.54	92.85	89.25	46.67	86.85	74.16	45.92
BIT [21]	75.87	80.89	82.03	83.12	90.48	41.26	88.09	90.36	47.68
ACC [10]	78.52	76.92	86.84	83.12	88.10	64.98	89.16	78.28	74.99
VA2M [23]	44.06	51.21	28.75	21.72	26.54	86.98	20.33	34.13	79.45
Challengers	81.22	77.01	66.06	86.42	69.33	79.67	87.38	55.60	72.77
T2									
NTNU [45]	90.68	84.57	85.41	77.29	80.60	91.58	94.02	94.09	85.03
HVRL [22]	97.35	98.07	95.45	97.63	98.82	96.72	100.00	97.66	87.96
BIT [21]	96.70	94.76	91.32	96.44	97.62	84.81	97.63	98.81	84.45
ACC [10]	96.70	95.43	91.27	91.58	96.41	98.33	97.62	85.61	100.00
VA2M [23]	64.33	60.41	62.96	60.99	66.21	61.30	71.90	76.75	28.02
T3									
NTNU [45]	68.81	73.70	59.39	66.02	69.14	65.08	79.75	61.12	59.94
HVRL [22]	55.45	55.34	53.57	59.62	61.70	47.47	53.77	58.29	42.17
BIT [21]	66.51	59.51	55.68	60.71	62.43	57.71	53.37	54.75	78.82

for containers 10 and 11, while BIT is the best for container 14. Containers 12 and 15 are the most challenging for BIT; container 14 for ACC; container 15 for HVRL; containers 10, 11, and 15 for NTNU. Challengers ranges between 55.60 \bar{F}_1 and 87.38 \bar{F}_1 across containers, with the drinking glasses being the most challenging and obtaining 69.33 \bar{F}_1 for container 11 and 55.60 \bar{F}_1 for container 14. For capacity estimation, NTNU achieves the best performance on containers 10 (66.02 \bar{C}), 11 (69.14 \bar{C}), 12 (65.02 \bar{C}), and 13 (79.75 \bar{C}), VA2M on container 14 (76.75 \bar{C}), and BIT on container 15 (78.82 \bar{C}). VA2M achieves higher average capacity score on the private cup and drinking glass than the public containers, but the score drops to 28.02 \bar{C} for the container 15. HVRL performs worse on the private testing containers than the public testing containers, with the lowest scores on the boxes (containers 12 and 15). Finally, BIT also performs worse for the drinking glass and cups in the private test set than the public test set. Surprisingly, the best score of BIT is on the *box* container 15 (78.82 \bar{C}) despite the modeled shape is a 3D cylinder. Current results show that it is still challenging to design a method that can generalize across the different containers and scenarios, especially for container capacity estimation and partially for filling level classification.

Finally, we discuss the overall performance of the methods based on their results on the challenge task of estimating the filling mass (see Tab. IX). ACC, Challengers, and NTNU addressed only two tasks out of three. Their final mass

TABLE IX
COMPARISON OF THE AVERAGE WEIGHTED SCORES FOR FILLING MASS ESTIMATION.

Method	Tasks			Test splits		
	T1	T2	T3	Public	Private	Overall
Random	●	●	●	38.47	31.65	35.06
ACC [10]	●	●	○	28.25	21.89	25.07
Challengers	●	●	○	29.25	23.21	26.23
NTNU [45]	○	●	●	38.56	39.80	39.18
VA2M [23]	●	●	●	52.80	51.14	53.47
HVRL [22]	●	●	●	63.32	61.01	62.16
BIT [21]	●	●	●	64.98	65.15	65.06

Accessed: 8 January 2021

estimation is complemented by the random results for the task that was not addressed and the score is weighted by the number of completed tasks. Methods addressing only filling type and level classification achieve a lower score than a random guess for each task. Given the multiplicative formula of the filling mass equation (see Eq. 2), even a few errors in these classification tasks can lead to a low score in the filling mass estimation, especially when combined with the random estimation of the container capacity. However, improving the capacity estimation is an important aspect to achieve more accurate results (and higher score) for the filling mass estimation (see NTNU). VA2M, HVRL, and BIT addressed all three tasks and achieved $53.47 \bar{M}$, $62.16 \bar{M}$, and $65.06 \bar{M}$, respectively. Overall, methods perform better on the public test set than the private test set, except for NTNU and BIT that achieve similar performance in the two test sets. We can observe that the more accurate predictions in the container capacity help VA2M to obtain $53.47 \bar{M}$ despite the classification errors for filling level and type. The high classification accuracy on filling level and type, combined with a similar score for the capacity estimations with respect to VA2M, makes HVRL and BIT the best performing in filling mass estimation. We can observe that container capacity and filling mass estimation have similar scores for the methods. This shows how important it is to accurately predict the capacity in order to correctly estimate the filling mass. Capacity estimation is therefore the most challenging task.

VII. CONCLUSION

We introduced a novel, open-access framework for the evaluation of multi-modal algorithms for the estimation of multiple physical properties of household containers manipulated by a person. Using this framework, we carried out an in-depth review and a comprehensive comparative analysis of several methods. The analysis showed that audio is a strong modality for solving the tasks of filling type and level classification, and it is also robust to changes in the container type, size, and shape, as well as pose during the manipulation. However, it is not yet clear how well audio-only methods can generalize to different environments and sensor setups [10]. Further research is also needed for the visual classification tasks. Current methods for estimating the container capacity rely on visual clues extracted from RGB, depth, or their combination. However, this task is still characterized by the large errors in

all methods, and also affects the estimation of other properties, such as filling mass. Finally, existing methods have mostly exploited the fixed camera views, while visual data acquired from the first-person camera worn by the subject was not much exploited. Severe occlusions and the motion of person could challenge even more the methods.

As future directions, we plan to include additional tasks such as the estimation of the container mass and the complete object weight, comprising both the container and content masses. We also plan to include additional modalities, such as tactile data from a robot hand moving to accomplish a hand-over. Lastly, the framework could be extended with data acquired from different sensors and environments to increase diversity as it is important to design multi-modal methods that can better exploit the complementary of modalities while overcoming their own limitations.

ACKNOWLEDGMENT

This work is supported by the CHIST-ERA program through the project CORSMAL, under UK EPSRC grant EP/S031715/1. We would like to thank Ricardo Sanchez-Matilla and Riccardo Mazzon for their contribution in the design and collection of the data, and the definition of the performance measures.

REFERENCES

- [1] R. Sanchez-Matilla, K. Chatzilygeroudis, A. Modas, N. Ferreira Duarte, A. Xompero, P. Frossard, A. Billard, and A. Cavallaro, "Benchmark for human-to-robot handovers of unseen containers with unknown filling," *IEEE Robotics Autom. Lett.*, vol. 5, no. 2, Apr. 2020.
- [2] J. R. Medina, F. Duvallet, M. Karnam, and A. Billard, "A human-inspired controller for fluid human-robot handovers," in *Proc. IEEE-RAS Int. Conf. Humanoid Robots*, Cancun, Mexico, 15–17 Nov. 2016.
- [3] P. Rosenberger, A. Cosgun, R. Newbury, J. Kwan, V. Ortenzi, P. Corke, and M. Grafinger, "Object-independent human-to-robot handovers using real time robotic vision," *IEEE Robotics Autom. Lett.*, vol. 6, no. 1, pp. 17–23, Jan. 2021.
- [4] V. Ortenzi, A. Cosgun, T. Pardi, W. P. Chan, E. Croft, and D. Kulić, "Object handovers: A review for robotics," *IEEE Trans. Robotics*, pp. 1–19, 2021.
- [5] W. Yang, C. Paxton, A. Mousavian, Y.-W. Chao, M. Cakmak, and D. Fox, "Reactive human-to-robot handovers of arbitrary objects," in *IEEE Int. Conf. Robotics Autom.*, 2021.
- [6] H. Liang, C. Zhou, S. Li, X. Ma, N. Hendrich, T. Gerkmann, F.-C. Sun, and J. Zhang, "Robust robotic pouring using audition and haptics," in *IEEE Int. Conf. Intell. Robot Syst.*, Las Vegas, NV, USA, 24 Oct. 2020–24 Jan. 2021.
- [7] A. Modas, A. Xompero, R. Sanchez-Matilla, P. Frossard, and A. Cavallaro, "Improving filling level classification with adversarial training," in *IEEE Int. Conf. Image Process.*, Anchorage, Alaska, USA, 19–22 Sep. 2021.
- [8] A. Xompero, R. Sanchez-Matilla, A. Modas, P. Frossard, and A. Cavallaro, "Multi-view shape estimation of transparent containers," in *IEEE Int. Conf. Acoustics, Speech Signal Process.*, Barcelona, Spain, 4–8 May 2020.
- [9] R. Mottaghi, C. Schenck, D. Fox, and A. Farhadi, "See the glass half full: Reasoning about liquid containers, their volume and content," in *IEEE Int. Conf. Comput. Vis.*, Venice, Italy, 22–29 Oct. 2017.
- [10] S. Donaher, A. Xompero, and A. Cavallaro, "Audio classification of the content of food containers and drinking glasses," in *Europ. Signal Proc. Conf.*, Virtual, 23–27 Aug. 2021.
- [11] C. Do and W. Burgard, "Accurate pouring with an autonomous robot using an RGB-D camera," in *Int. Conf. Intell. Auton. Syst.*, Baden-Baden, Germany, 12–16 Jul. 2018.
- [12] C. Schenck and D. Fox, "Reasoning about liquids via closed-loop simulation," in *Robotics: Science and Syst.*, Cambridge, Massachusetts, USA, 12–16 Jul. 2017.

- [13] H. Liang, S. Li, X. Ma, N. Hendrich, T. Gerkmann, F. Sun, and J. Zhang, "Making sense of audio vibration for liquid height estimation in robotic pouring," in *IEEE Int. Conf. Intell. Robot Syst.*, Macau, China, Nov. 2019.
- [14] S. Sajjan, M. Moore, M. Pan, G. Nagaraja, J. Lee, A. Zeng, and S. Song, "ClearGrasp: 3D shape estimation of transparent objects for manipulation," in *IEEE Int. Conf. Robotics Autom.*, 2020.
- [15] T. Hodaň, F. Michel, E. Brachmann, W. Kehl, A. Glent Buch, D. Kraft, B. Drost, J. Vidal, S. Ihrke, X. Zabulis, C. Sahin, F. Manhardt, F. Tombari, T.-K. Kim, J. Matas, and C. Rother, "BOP: Benchmark for 6D object pose estimation," in *Eur. Conf. Comput. Vis.*, Munich, Germany, 8–14 Sep. 2018.
- [16] R. Kaskman, S. Zakharov, I. Shugurov, and S. Ilic, "Homebreweddb: RGB-D dataset for 6D pose estimation of 3D objects," in *IEEE Int. Conf. Comput. Vis. Workshops*, Seoul, Korea, 27 Oct./2 Nov. 2019.
- [17] X. Liu, R. Jonschkowski, A. Angelova, and K. Konolige, "Keypose: Multi-view 3d labeling and keypoint estimation for transparent objects," in *IEEE Conf. Comput. Vis. Pattern Recognit.*, Virtual, 14–19 Jun. 2020.
- [18] X. Chen, Z. Dong, J. Song, A. Geiger, and O. Hilliges, "Category level object pose estimation via neural analysis-by-synthesis," *arXiv preprint arXiv:2008.08145*, 2020.
- [19] D. Chen, J. Li, Z. Wang, and K. Xu, "Learning canonical shape space for category-level 6D object pose and size estimation," in *IEEE Conf. Comput. Vis. Pattern Recognit.*, Virtual, 14–19 Jun. 2020.
- [20] H. Wang, S. Sridhar, J. Huang, J. Valentin, S. Song, and L. J. Guibas, "Normalized object coordinate space for category-level 6d object pose and size estimation," in *IEEE Conf. Comput. Vis. Pattern Recognit.*, Long Beach, CA, USA, 16–20 Jun. 2019.
- [21] V. Iashin, F. Palermo, G. Solak, and C. Coppola, "Top-1 CORSMAL challenge 2020 submission: Filling mass estimation using multi-modal observations of human-robot handovers," in *IEEE Conf. Pattern Recognit. Workshops and Challenges*, Virtual, 10–15 Jan. 2021.
- [22] R. Ishikawa, Y. Nagao, R. Hachiuma, and H. Saito, "Audio-visual hybrid approach for filling mass estimation," in *IEEE Conf. Pattern Recognit. Workshops and Challenges*, Virtual, 10–15 Jan. 2021.
- [23] Q. Liu, F. Feng, C. Lan, and R. H. M. Chan, "VA2Mass: Towards the fluid filling mass estimation via integration of vision & audio learning," in *IEEE Conf. Pattern Recognit. Workshops and Challenges*, Virtual, 10–15 Jan. 2021.
- [24] C. Do, T. Schubert, and W. Burgard, "A probabilistic approach to liquid level detection in cups using an RGB-D camera," in *IEEE Int. Conf. Intell. Robot Syst.*, Daejeon, Korea, 9–14 Oct. 2016.
- [25] K. He, G. Gkioxari, P. Dollár, and R. B. Girshick, "Mask R-CNN," in *IEEE Int. Conf. Comput. Vis.*, Venice, Italy, 22–29 Oct. 2017.
- [26] S. Griffith, V. Sukhoy, T. Wegter, and A. Stoytchev, "Object categorization in the sink : Learning behavior – grounded object categories with water," in *IEEE Int. Conf. Robotics Autom.*, Minneapolis, MN, USA, 14–18 May 2012.
- [27] S. Ikeno, R. Watanabe, R. Okazaki, T. Hachisu, M. Sato, and H. Kajimoto, "Change in the amount poured as a result of vibration when pouring a liquid," in *Int. AsiaHaptics Conf.*, Tsukuba, Japan, 18–20 Nov. 2014.
- [28] S. Clarke, T. Rhodes, C. Atkeson, and O. Kroemer, "Learning audio feedback for estimating amount and flow of granular material," in *Proc. Conf. Robot Learn.*, Zürich, Switzerland, 29–31 Oct. 2018.
- [29] K. J. Piczak, "Environmental sound classification with convolutional neural networks," in *Proc. Int. Workshop Mach. Learning Signal Process.*, 2015.
- [30] J. Salamon and J. Bello, "Deep convolutional neural networks and data augmentation for environmental sound classification," *IEEE Signal Process. Letters*, vol. 24, pp. 279–283, 2017.
- [31] S. Dieleman, P. Brakel, and B. Schrauwen, "Audio-based music classification with a pretrained convolutional network," in *ISMIR*, 2011.
- [32] T. Cover and P. Hart, "Nearest neighbor pattern classification," *IEEE Trans. Inf. Theory*, vol. 13, pp. 21–27, 1967.
- [33] C. Cortes and V. Vapnik, "Support-vector networks," *Machine Learning*, vol. 20, pp. 273–297, 1995.
- [34] L. Breiman, "Random forests," *Machine Learning*, vol. 45, pp. 5–32, 2004.
- [35] K. He, X. Zhang, S. Ren, and J. Sun, "Deep residual learning for image recognition," in *IEEE Conf. Comput. Vis. Pattern Recognit.*, Las Vegas, NV, USA, 27–30 Jun. 2016.
- [36] D. Tran, H. Wang, L. Torresani, J. Ray, Y. LeCun, and M. Paluri, "A closer look at spatiotemporal convolutions for action recognition," in *IEEE Conf. Comput. Vis. Pattern Recognit.*, Salt Lake City, Utah, USA, 18–22 Jun. 2018.
- [37] L. Bossard, M. Guillaumin, and L. Van Gool, "Food-101 – mining discriminative components with random forests," in *Eur. Conf. Comput. Vis.*, Zurich, Switzerland, 16–12 Sep. 2014.
- [38] Y. Kawano and K. Yanai, "FoodCam-256: A large-scale real-time mobile food recognition system employing high-dimensional features and compression of classifier weights," in *ACM Int. Conf. Multimedia*, Orlando, Florida, USA, 3–7 Nov. 2014.
- [39] H. Zhao, K.-H. Yap, and A. C. Kot, "Fusion learning using semantics and graph convolutional network for visual food recognition," in *IEEE Winter Conf. Appl. Comput. Vis.*, Jan. 2021.
- [40] K. Simonyan and A. Zisserman, "Very deep convolutional networks for large-scale image recognition," in *Int. Conf. Learning Represent.*, Banff, Canada, 14–16 Apr. 2014.
- [41] A. Xompero, R. Sanchez-Matilla, R. Mazzon, and A. Cavallaro, "CORSMAL Containers Manipulation," 2020, (1.0) [Data set]. Queen Mary University of London. [Online]. Available: http://cormsal.eecs.qmul.ac.uk/containers_manip.html
- [42] H. Yang and L. Carlone, "In perfect shape: certifiably optimal 3d shape reconstruction from 2d landmarks," in *IEEE Conf. Comput. Vis. Pattern Recognit.*, Seattle, Washington, USA, 16–18 Jun. 2020.
- [43] A. Ahmadyan, L. Zhang, J. Wei, A. Ablavatski, and M. Grundmann, "Objectron: A large scale dataset of object-centric videos in the wild with pose annotations," *arXiv preprint arXiv:2012.09988*, 2020.
- [44] C. J. Phillips, M. Lecce, and K. Daniilidis, "Seeing glassware: from edge detection to pose estimation and shape recovery," in *Robotics: Science and Syst.*, Ann Arbor, Michigan, USA, 18–22 Jun. 2016.
- [45] G. Christmann and J.-T. Song, "2020 CORSMAL Challenge - Team NTNU-ERCReport," 2020. [Online]. Available: <https://github.com/guichristmann/CORSMAL-Challenge-2020-Submission/blob/master/PaperReport.pdf>
- [46] J. Deng, W. Dong, R. Socher, L.-J. Li, L. Li, and L. Fei-Fei, "ImageNet: A large-scale hierarchical image database," in *IEEE Conf. Comput. Vis. Pattern Recognit.*, Jun. 2009.
- [47] F. T. Liu, K. M. Ting, and Z.-H. Zhou, "Isolation forest," in *Proc. IEEE Int. Conf. Data Mining*, Pisa, Italy, 15–19 Dec. 2008.
- [48] R. Hartley and A. Zisserman, *Multiple View Geometry in Computer Vision*, 2nd ed. Cambridge University Press, 2003.
- [49] D. P. Kingma and J. Ba, "Adam: A method for stochastic optimization," in *Int. Conf. Learning Represent.*, San Diego, CA, USA, 7–9 May 2015.
- [50] N. Srivastava, G. E. Hinton, A. Krizhevsky, I. Sutskever, and R. Salakhutdinov, "Dropout: a simple way to prevent neural networks from overfitting," *J. Mach. Learn. Res.*, vol. 15, pp. 1929–1958, 2014.
- [51] S. Ioffe and C. Szegedy, "Batch normalization: Accelerating deep network training by reducing internal covariate shift," in *Int. Conf. Mach. Learning.*, Jul. 2015.
- [52] A. Bochkovskiy, C. Wang, and H. M. Liao, "YOLOv4: Optimal speed and accuracy of object detection," *arXiv:2004.10934 [cs.CV]*, 2020.
- [53] T.-Y. Lin, M. Maire, S. Belongie, J. Hays, P. Perona, D. Ramanan, P. Dollár, and C. L. Zitnick, "Microsoft COCO: Common objects in context," in *Eur. Conf. Comput. Vis.*, Munich, Germany, 8–14 Sep. 2018.
- [54] S. Hershey, S. Chaudhuri, D. P. W. Ellis, J. F. Gemmeke, A. Jansen, R. C. Moore, M. Plakal, D. Platt, R. A. Saurous, and B. Seybold, "CNN architectures for large-scale audio classification," in *IEEE Int. Conf. Acoustics, Speech Signal Process.*, 2017.
- [55] J. F. Gemmeke, D. P. W. Ellis, D. Freedman, A. Jansen, W. Lawrence, R. C. Moore, M. Plakal, and M. Ritter, "Audio Set: An ontology and human-labeled dataset for audio events," in *IEEE Int. Conf. Acoustics, Speech Signal Process.*, New Orleans, LA, 2017.
- [56] J. Chung, C. Gulcehre, K. Cho, and Y. Bengio, "Empirical evaluation of gated recurrent neural networks on sequence modeling," in *Adv. Neural Inf. Process. Syst. Workshop Deep Learning*, 2014.
- [57] W. Kay, J. Carreira, K. Simonyan, B. Zhang, C. Hillier, S. Vijayanarasimhan, F. Viola, T. Green, T. Back, P. Natsev, M. Suleyman, and A. Zisserman, "The Kinetics human action video dataset," *arXiv:1705.06950 [cs.CV]*, 2017.
- [58] B. McFee, C. Raffel, D. Liang, D. Ellis, M. McVicar, E. Battenberg, and O. Nieto, "librosa: Audio and music signal analysis in python," in *Proc. Python in Science Conf.*, 2015.
- [59] M. Matsumoto and T. Nishimura, "Mersenne twister: A 623-dimensionally equidistributed uniform pseudo-random number generator," *ACM Trans. Model. Comput. Simul.*, vol. 8, no. 1, p. 3–30, Jan. 1998.